Published in final edited form as:
Aquat Toxicol. 2019 November ; 216: 105297. doi:10.1016/j.aquatox.2019.105297.

Effects of graphene oxide nanomaterial exposures on the marine bivalve, *Crassostrea virginica*

Bushra Khan[1,*], **Adeyemi S. Adeleye**[1,†], **Robert M. Burgess**[2], **Stephen M. Russo**[3], **Kay T. Ho**[2]

[1]National Research Council Postdoctoral Research Associate at the US Environmental Protection Agency, ORD-NHEERL, Atlantic Ecology Division, 27 Tarzwell Drive, Narragansett, RI 02882

[2]US Environmental Protection Agency, ORD-NHEERL, Atlantic Ecology Division, 27 Tarzwell Drive, Narragansett, RI 02882

[3]Oak Ridge Associated Universities Student Services Contractor at the US Environmental Protection Agency, ORD-NHEERL, Atlantic Ecology Division, 27 Tarzwell Drive, Narragansett, RI 02882

Abstract

Since its discovery in 2004, graphene has been used in a wide variety of fields including biomedicine, electronics, filtration materials, and surface coatings. The rapidly expanding consumer market for graphene family nanomaterials (GFNs), such as graphene oxide (GO), raises concern regarding their environmental toxicity. The aim of this study was to evaluate the effects of GO exposures in a marine filter-feeding bivalve (*Crassostrea virginica*) using sublethal biomarker approaches that can contribute to the development of an adverse outcome pathway (AOP). A 14-day study was conducted to identify tissue-specific molecular markers of GO toxicity using a static renewal design. Elevated lipid peroxidation and changes in glutathione-s-transferase (GST) activities were observed in gills and digestive gland tissues of the GO-exposed oysters. These cellular changes were noted for 2.5 and 5 mg/L GO exposures in seawater. Based on our results, reactive oxygen species (ROS)-induced oxidative damage is identified as a key event in the proposed AOP. Additionally, detoxification enzymes, such as GST, are thought to be involved in stress signaling leading to adverse effects on cellular health. This study is a part of our two-tier

*corresponding author: Bushra Khan, khan.bushra@epa.gov.
†Current address: Department of Civil & Environmental Engineering, University of California-Irvine, Irvine, CA 92697

Declaration of interest: none

Disclaimer
The views expressed in this article are those of the authors and do not necessarily reflect the views or policies of the U.S. Environmental Protection Agency (EPA). Mention of trade names and products does not imply an endorsement or recommendation for use by the U.S. Government or the U.S. EPA. The present study is number ORD- 029966 of the Atlantic Ecology Division of the U.S. EPA, Office of Research and Development, National Health and Environmental Effects Research Laboratory.

Data Availability
Readers can access much of the data and statistical assessments in the Supplemental Information (SI). Additional data and supporting information are available on request (khan.bushra@epa.gov).

approach towards the identification of short- and long-term effects of GO exposures. This work, together with our previous 72 h exposure, represents the application of biomarker-based investigations in the process of AOP development for graphene family nanomaterials.

Keywords

Graphene oxide; carbon nanomaterials; nanotoxicity; adverse outcome pathways; oysters; bivalves

1. Introduction

Graphene is a two-dimensional nanomaterial that is known for its unique properties and use in a variety of applications such as electronics, composite materials, and biomedicine (Adeleye et al. 2016; Huang et al. 2011; Novoselov et al. 2012). Graphene oxide (GO) is a graphene family nanomaterial (GFN) with rapidly increasing use in biomedical and industrial applications due to its reliable aqueous dispersibility and colloidal stability (Bitounis et al. 2013; Qi et al. 2015). Use of GO in applications such as aqueous pollutant degradation and drinking water treatment, along with disposal of GO-containing products including coating materials and desalination membranes, could lead to its release into coastal and marine habitats (Zhu et al. 2017). Although some reports on GO toxicity are available, our understanding of the environmental risks associated with such exposures to aquatic organisms remains limited. Zebrafish studies have reported GO-induced immunotoxicity, oxidative stress, and structural damage to liver and intestinal tissues (Chen et al. 2016; Souza et al. 2017). Changes in swimming behavior and enzyme biomarkers in *Artemia* larvae along with mortality at high concentration (700 mg/L) have been shown after 48 h of GO exposures (Mesarič et al. 2015). In a wastewater microbial community, metabolic activity was found to be inhibited at ≥10 mg/L and decreased viability was reported at ≥50 mg/L GO (Ahmed and Rodrigues 2013). *In vitro* GO exposure of *Mytilus* hemocytes has been shown to adversely affect cell viability and membrane integrity and increase reactive oxygen species (ROS) production (Katsumiti et al. 2017). Apart from the *Mytilus* study reported by Katsumiti et al and our studies with *Crassostrea* (Khan et al. 2019), effects of GO on marine bivalves have not been previously reported.

In seawater, GO agglomerates and gradually settles out of the water column (Adeleye et al. 2019). Benthic marine bivalves are unique targets of nanomaterial toxicity due to their filter-feeding capacities and physiological functions, such as intracellular digestion (Canesi et al. 2012). Bivalves feed by capturing particulate matter from the water column using their gills as sieves. Further, particle size affects capturing efficiency and it has been shown that nanomaterial incorporated into agglomerates are more efficiently captured by bivalves than individual free suspended particles. Therefore, agglomeration of nanomaterial and their incorporation into larger particle masses can increase nanomaterial bioavailability to marine bivalves (Ward and Kach 2009), thereby making them good candidates for GO toxicity studies.

Oxidative stress has been reported as one of the main underlying mechanisms of toxic effects of nanomaterials including GFNs (Nel et al. 2006; Sanchez et al. 2011; Souza et al.

2017). Cellular ROS production in healthy cells is controlled by antioxidants, such as glutathione, catalase, superoxide dismutase, and glutathione peroxidase. However, elevated ROS production due to contaminant exposures and/or tissue injury can overwhelm the antioxidant and detoxification machinery, cause oxidative stress, and result in cyto- and geno-toxicity (Guo and Mei 2014). Oxidation of polyunsaturated fatty acids (PUFAs), a component of cellular membranes, produces a variety of oxidized products including malondialdehyde (MDA) which is often used as a stress marker of ROS-induced cellular lipid damage (Kelly et al. 1998; Khan and Ringwood 2016; McCarthy et al. 2013; Sayes et al. 2005). Lipid peroxidation is a self-propagating chain reaction and its increased rates may reflect excessive production of ROS. Glutathione (GSH), a thiol antioxidant, serves as the first line of defense against such damage, scavenges ROS, and consequently gets oxidized to glutathione disulfide (GSSG). Additionally, enzymatic conjugation of glutathione to a wide variety of electrophilic compounds, such as therapeutic drugs, environmental toxins, and oxidative damage products, is facilitated by glutathione-s-transferases (GSTs) as a detoxification mechanism. Along with their role in phase II detoxification and maintenance of the thiol pool, the GST enzyme family also has antiperoxidative properties and signaling functions (Tew and Townsend 2012). The role of GST in nanotoxicity is important to consider due to such multifold functions in cellular pathways (Chae et al. 2009; Shi et al. 2012). As markers of contaminant stress, both lipid peroxidation and GST offer insights into potential stress responses and lay the foundation for identification of exposure effects.

The current study was designed as a tier-2 long-term (14 d) exposure, preceded by our recent tier-1 short-term (72 h) preliminary study (Khan et al. 2019), to identify GO-induced cellular responses using Eastern oysters (*C. virginica*) as a model. Biomarker assessments, as presented here, are important for the development of adverse outcome pathways (AOPs). An AOP is a representation of linked events at different levels of biological organization such that a molecular initiating event (MIE) is connected to an adverse outcome (AO) via a series of key events (KEs) (Ankley et al. 2010). In an AOP framework, the initial events are identified at lower levels of organization (i.e., measurable molecular and cellular changes, also called biomarkers) and they lead to an AO that is relevant to risk assessment (e.g., individual mortality, population impacts). Introduction of the concept of AOPs as an information tool has allowed us to understand the implications of biomarker research in environmental risk assessment and regulatory decision making (Lee et al. 2015). Although *in vitro* screening and cell based assays offer a rapid tier-1 screening for the identification of contaminants' mode of action and are useful in detecting sublethal effects in aquatic organisms (Volz et al. 2011), they lack the physiological complexity of an intact organism, as well as eco-bio-interactions (Canesi and Corsi 2016; Yozzo et al. 2013). There is limited understanding of GO behavior in complex natural matrices, and little is known about its environmental portioning, fate upon entering the organism and tissue distribution. Based on the current challenges and requirements in the area of graphene family nanotoxicity, we conducted a set of *in vivo* GO exposures towards the overall goal of contributing biomarker-based information to an AOP framework for an emerging contaminant.

2. Materials and methods

2.1 GO Characterization

GO suspension dispersed in deionized (DI) water was purchased from Cheap Tubes Inc. (5 g/L, few layered GO, >99 wt % purity, 300–800 nm). The GO used for conducting this exposure was similar to what we had used in our 72 h study. A detailed characterization has been described previously (Khan et al. 2019). X-ray photoelectron spectroscopy (XPS) was performed to determine functional groups on the surface of pristine GO powder using a Perkin-Elmer 550 Multi-technique Surface Analyzer. GO was visualized in its pristine state via scanning electron microscopy (SEM) with a ZEISS Sigma VP field emission-scanning electron microscope. Evaluation of surface charge (zeta (ζ) potential measurement) and effective diameter (hydrodynamic size measurement) were performed with a Brookhaven ZetaPALS potential analyzer using dynamic light scattering (DLS) technique.

2.2 Experimental design

Oysters (6.6 ± 0.4 cm long, 4.7 ± 0.4 cm wide) were provided by Matunuck Oyster Farm, RI, USA, acclimated in the laboratory for five days and fed a mixed algal diet (75 mL/oyster) consisting of *Tetraselmis*, *Pavlova*, *Chaetoceros*, and *Thalassiosira*. Algal cultures were maintained at 10^6-10^7 cells/mL. Three sets of nine glass chambers were placed in three water tables (27 chambers total) to test the effects of control (0 mg/L), 2.5 mg/L and 5 mg/L GO using a static renewal exposure design. Currently, no environmentally relevant concentrations of GO are available. The test concentrations were chosen based on our preliminary study (Khan et al. 2019) as well as other reports on GO toxicity (Chang et al. 2011; Katsumiti et al. 2017; Souza et al. 2017; Zhu et al. 2017). A water bath in each table was used to maintain the temperature at about 20 °C and all chambers were aerated. One oyster was introduced per chamber along with 0.22 μm filtered natural seawater (Narragansett Bay, RI) to the first eight chambers in each table (n = 8 oysters per treatment). The remaining one chamber in each table was used as a seawater (SW)-only chamber to assess GO concentration and size over time. A working suspension of 500 mg/L GO at 30 ‰ salinity was prepared by mixing 120 mL DI water, 60 mL brine (100 ‰) and 20 ml GO (5 g/L). The working suspension was probe-sonicated for 20 min using a Branson 250 sonicator. Immediately following sonication, GO was added to the chambers sequentially to obtain final concentrations of 2.5 and 5 mg/L; no GO was added to the control chambers. The final volume of each chamber was maintained at 1 L. Two complete renewals of GO and water were performed daily (10:00 and 16:00) using freshly prepared working suspension of GO for a total exposure duration of 14 days. Control chambers received two seawater renewals daily. All chambers were maintained on a cycle of 16 h of light and 8 h of dark. Temperature, salinity, and dissolved oxygen readings were recorded using a YSI meter and oysters were fed 75 mL of mixed algal diet every morning 1.5 h before the first GO renewal for the day. At the end of 14 days of exposure, oysters were moved to chambers with 1 L of 0.22 μm filtered natural seawater for 2 h. Oysters were then sacrificed, and gills and digestive gland tissues were harvested and immediately stored in a pre-chilled cryotube at −80 °C for biochemical analyses as described in section 2.4.

2.3 Exposure water assessments for GO size and concentration

Five sets of samplings were conducted to obtain exposure chamber nanomaterial size and concentration measurements. Each set was three days apart and was comprised of three chambers (two with oysters and one without oyster) per concentration sampled before and after the first GO renewal in the morning. For each measurement, water samples (about 2.5 mL) were collected using glass Pasteur pipettes from the immediate surroundings of the oyster (about 2–3 cm from the bottom of the chambers) 2 min after GO addition to the chambers started. Out of the 2.5 mL water samples, 1 mL was used for DLS analyses measured with a Zeta PALS instrument. For the DLS analyses, the autocorrelation function was allowed to accumulate for 2 min per measurement and a 4-min interval was maintained between each analysis to ensure that the time between sample collection and measurement was consistent for each sampling set. DLS readings with a polydispersity index (PDI) ≥0.4 were discarded to obtain reliable particle size assessments. The ZetaPALS instrument's incident power was set such that it did not self-optimize for each sample (run after the first one which was kept at about 500 kilo counts per second). This insured that the average count rate value provided could be used as an indicator of particle count/density. Following the DLS analysis, the remaining sample was utilized for GO concentration assessments using a Biotek Synergy HTX multimode reader. Samples were shaken and placed in duplicate in a 96-well microplate (200 μL in each well) and absorbance measured immediately at 230 nm. Count rates and concentration assessments together were used to identify differences between chambers over time.

2.4 Biochemical Analyses

2.4.1 Lipid peroxidation—Lipid peroxidation was estimated using a commercial kit (MAK085) purchased from Sigma-Aldrich by measuring MDA levels. MDA is one of the secondary products of lipid peroxidation and its levels indicate relative oxidative damage in tissues. The kit uses thiobarbituric acid (TBA) and relies on the formation of a colored adduct of TBA and MDA which is detected spectrophotometrically at 532 nm. The endpoint colorimetric assay was performed using about 25 to 45 mg of frozen tissue that was homogenized in lysis buffer containing 1% butylated hydroxytoluene. Homogenates were kept cool on ice and centrifuged at 13,000 *g* for 10 min. Supernatants (100 μL) were mixed with TBA (600 μL) and incubated at 95 °C for an hour. Following the incubation, samples were cooled to room temperature, and centrifuged at 13,000 *g* for 5 min. Supernatants were read in duplicate on the BioTek Synergy HTX multimode reader using Gen5 3.02 software.

2.4.2 Glutathione-s-transferase activity—GST activity was measured using a commercial kit (CS0410) purchased from Sigma-Aldrich. The spectrophotometric kinetic assay relies on GST-mediated conjugation of 1-chloro-2,4-dinitrobenzene (CDNB) to glutathione. Elevated GST activity represents a detoxification response to chemical stress that may also affect stress-mediated signaling (Lushchak 2012). Frozen oyster tissue samples (25 to 45 mg) were homogenized in lysis buffer (containing protease inhibitor cocktail) on ice and centrifuged at 10,000 *g*, 4 °C for 15 min. Supernatants were diluted and 10 μL of each diluted sample were added in duplicate to a 96-well microplate. A mix of reduced L-glutathione, CDNB and phosphate buffered saline was added sequentially to the samples in the wells and six kinetic readings were recorded to generate reaction curves using

Gen5 3.02 on the BioTek Synergy HTX multimode reader. The conjugation of CDNB to the thiol group of glutathione leads to a change in absorbance at 340 nm which is used to quantify enzyme activities. Diluted GST controls were run with every set of assessments.

2.4.3 Total protein—Protein levels were estimated using a modified Bradford assay that utilizes the change in absorbance from 465 nm to 595 nm upon binding of Coomassie dye to the proteins in the sample in an acidic medium. Protein levels are used to normalize enzyme biomarker data and indicate overall cellular health. The assay was performed using a protein assay kit (PI23200) and bovine serum albumin standards (PI23209) from Thermo Scientific. The dye (250 μL) was added to the homogenized sample (10 μL, from the homogenate used for the GST activity assay, section 2.4.2) in duplicate in a 96-well microplate. The plate was shaken for 30 sec to allow mixing, followed by incubation for 10 min at room temperature. Samples were read on the Biotek Synergy HTX multimode reader and a standard curve was generated using a four-parameter (quadratic) algorithm in Gen5 3.02 software.

2.5 Statistical analyses

Sigma Plot 13.0 statistical software was used to perform analysis of variance (ANOVA) and two-tailed t-tests. Statistical significance was identified at $p \leq 0.05$ and significant ANOVA were followed by the Student-Newman-Keuls (SNK) pairwise multiple comparison post-hoc test. The Shapiro-Wilk normality test and Brown-Forsythe equal variance tests were conducted on each set of data to confirm normal distribution and equal variance assumptions, respectively. Datasets that violated these assumptions were compared using non-parametric tests such as the Mann-Whitney Rank Sum test. Detailed results from all statistical comparisons are included in the supplementary information. Values in all associated graphs represent means and standard deviations.

3. Results

3.1 GO characterization

According to the manufacturer, each discreet GO particle is made up of 2–4 layers (equivalent to about 1.4 – 2.8 nm thickness) and the lateral size of the particle is 300 – 700 μm. The effective size and ζ potential of GO were 639 nm and −37 mV, respectively, in DI water. Figures 1A and 1B show a scanning electron micrograph of GO agglomerates, and carbon to oxygen ratios obtained from the XPS analyses, respectively. The carbon (60.7%) to oxygen (39.3%) ratio was 1.5 (Figure 1B), which is typical for GO (Goodwin et al. 2018). GO has a negative surface charge due to the ionization of its functional groups (mainly OH and COOH). These functional groups were identified by deconvoluting the C1s spectra obtained using the XPS analysis as reported in our previous study (Khan et al. 2019). The stability of GO in DI can be attributed to the electrostatic repulsion between particles resulting from the nanomaterial's surface charge (Adeleye et al. 2019; Goodwin et al. 2018).

3.2 Exposure water assessments

Average temperature, salinity, and dissolved oxygen in the chambers were 19.7 ± 0.4 °C, 30.9 ± 0.5 ‰, and 7.5 ± 0.2 mg/L, respectively. The mean GO concentration in the first 35 minutes of GO addition to the 2.5 mg/L chambers was 1.3 mg/L and 1.2 mg/L, with and

without oysters, respectively. For 5 mg/L chambers, GO concentration with and without oysters was 3.0 mg/L and 2.8 mg/L, respectively. These measured concentrations indicate no significant differences between the chambers with and without oysters (Figure 2A, Table S1). However, at the end of 16 hours of exposure, significant differences between chambers with and without oysters were noted for both test concentrations (Figure 2B, Table S1). In chambers with oysters, no GO was detected at the end of 16 hours for either test concentration.

Similar to GO concentration measurements, the average count rate showed no significant differences between chambers with and without oysters within the initial 35 minutes (Figure 3A, Table S2). At the end of 16 hours, the average count rate was significantly higher in the chambers without oysters for both test concentrations (Figure 3B, Table S2).

The mean effective diameter of GO in the first 35 minutes had reached about 3 μm in chambers with oysters and about 4 μm in chambers without oysters (Figure 4). These effective diameter measurements were not significantly different (Table S3).

The size distribution table shows a variety of particle sizes present in the water column ranging from nano to micron size range (Table 1). The most abundant size present in the water for test concentrations was less than a micron, ranging from 68 to 316 nm for chambers with oysters. It must be noted that the particles which represent the bulk of the data (frequency >1, represented by particles scoring above 1 on a distribution scale where the most abundant sized particle is assigned a value of 100 relative units) ranged between less than 100 nm to less than 2 μm as seen in Table 1. Most of the chambers showed a narrower range of particles not exceeding a micron. The mean effective diameter as shown in Table 1 represents the intensity-averaged sizes of all the particles detected in each sample by the ZetaPALS. Less abundant (scoring <1 on the distribution scale) particles with sizes in the micron range are also included in Table 1 (included in the ‘all data’ column under ‘size range’). The upper detection limit reported by the ZetaPALS is 10,000 nm, and the large (micron-sized) particles, though few, are strongly reflected in the effective diameter measurements.

3.3 Biomarker assessments

3.3.1 Lipid peroxidation assay—Lipid peroxidation, quantified as MDA, was higher in GO-exposed oysters than controls. As presented in Figure 5 (Tables S4 and S5), significantly elevated levels of MDA were found in gills and digestive glands of oysters exposed to 2.5 and 5 mg/L GO. No significant differences were noted between 2.5 and 5 mg/L exposure groups. Figure 5 shows nmol of MDA expressed per gram of wet tissue (Figure 5A) as well as normalized to per mg protein in the tissues (Figure 5B). Regardless of how the data were computed, both Figure 5A and B show the same pattern of increase in MDA levels. Overall, digestive gland tissues have higher MDA levels, including baseline control values.

3.3.2 Glutathione-s-transferase assay—GST activities were also expressed as per gram wet tissue weight (Figure 6A) as well as per mg protein (Figure 6B). Elevated GST activity was observed in GO-exposed oysters for both test concentrations. Significant

increases in GST activity in oyster gills were only noted when the data were normalized to the total tissue protein levels (Figure 6B, Tables S6 and S7) and no differences were found between 2.5 and 5 mg/L GO-exposed groups. In the digestive gland tissues, the highest GST activity was found in oysters exposed to the 2.5 mg/L exposure concentration. Again, the patterns of changes in GST activities were found to be similar regardless of how the data are presented (i.e., expressed per gram of wet tissue weight or per mg protein (Figures 6A and 6B)).

3.3.3 Total protein assay—No differences were observed in the protein levels between control and GO-exposed oysters for gill or digestive gland tissues (Figure 7, Table S8).

4. Discussion

4.1 Exposure water assessments

For the initial measurements taken within the first 35 minutes, GO concentrations were found to be similar between chambers with and without oysters. Once GO is introduced into the chambers, the concentration is expected to decrease due to filtration by the oyster, adherence to surfaces (such as the chamber wall, aeration tubing, oyster shell), and sedimentation. Our 16 h measurements, as shown in Figures 2 and 3, reflect the differences between chambers with and without oysters. The average count rate in the chambers without oysters remained unchanged even after 16 h suggesting that a significant portion of the particles was actively removed by the oysters and/or the presence of the oyster resulted in adherence of GO to the shell. For the control chambers, the absorbance readings at 230 nm were comparable to blank (0.22 μm filtered seawater) measurements. Due to the presence of organic matter, the blank absorbance readings and the y-intercept values, generated from a standard curve for GO suspended in filtered seawater, were above zero. These readings were used to obtain measurements as seen in Figure 2 and the control concentrations below zero are reflective of the positive y-intercept. Further, even though the GO concentration measurements in the control chambers are below zero, the count rate is a non-zero number (≤28) and likely also reflects the suspended natural organic matter in the water column. Such environmentally relevant seawater parameters are essential to consider for nanotoxicity studies. Interestingly, similar to the results from our previous 72 h study (Khan et al. 2019), a wide range of particle sizes were detected in the exposure chambers as shown in Table 1. GO is negatively charged and its aggregation is encouraged by the presence of positively charged ions in seawater (Adeleye et al. 2019; Chowdhury et al. 2013). Environmental exposures to nanomaterials are most likely characterized by heterogenous suspensions due to particle interactions and association with organic matter in the water column. Such associations could affect particle size, as seen in our study, and result in changes in bioavailability and uptake mechanisms by filter-feeders. We found the most abundant sized particles to be much smaller (over an order of magnitude) than the effective diameter and the majority of the particles (represented as frequency >1) sized below a micron in our exposure chambers. In bivalves, cellular uptake of suspended particles is performed by endocytotic (for nanoscale particles) and phagocytotic (microscale particles) mechanisms (Moore 2006). Further, size-dependent cellular uptake of protein-coated GO via such pathways has been reported (Mu et al. 2012). Based on our DLS data, we suggest that GO agglomerates were in

the size range that could be taken up by the oysters. Further, the mechanisms of uptake and the fate of GO agglomerates upon entry in oysters are likely multifaceted. Particle size assessments in the exposure chambers, such as presented in the current study, are critical for understanding potential nanomaterial bioavailability and uptake processes. It must be noted that quantification of GO in the exposed organisms is difficult due to the limited availability of analytical techniques for detecting carbonaceous nanomaterials in biological matrices (Goodwin et al. 2018). Therefore, there is a current need to develop such quantification techniques to improve our understanding of GFN bioavailability and toxicity.

4.2 Biomarker assessments

4.2.1 Lipid peroxidation—Although a few recent GO studies have reported elevated lipid damage (De Marchi et al. 2017; Wang et al. 2014), no information on tissue-specific patterns of such effects in molluscs is currently available. We observed elevated MDA levels in gill and digestive gland tissues of GO-exposed oysters, suggesting ROS-induced lipid peroxidation. Overall, MDA levels in the gills were lower than digestive glands. Such tissue-specific differences in baseline MDA levels, as seen in Figure 5 (controls), are indicative of differences in antioxidant potential (Regoli and Principato 1995). However, for both tissues, no further increases were noted at the highest concentration. It is possible that sustained elevated GST activities, as seen in our studies, as well as other antioxidant enzymes, and compensatory mechanisms prevented further increases in lipid peroxidation at the highest concentration. It must be noted that GSTs can reduce hydroperoxides and other products of lipid peroxidation such as 4-hydroxynonenal (HNE) (Awasthi et al. 2004; Kalinina et al. 2014). Accumulation of intracellular ROS, which is reflective of oxidative stress, has been proposed as one of the key mechanisms of GFN toxicity (Chang et al. 2011; Jastrzębska et al. 2012; Lammel and Navas 2014; Li et al. 2012). However, generation of ROS can be due to direct physical interaction of the nanomaterial with cellular membranes or indirect cellular response following exposure (Jastrzębska et al. 2012; Sanchez et al. 2011). Surface oxidative reactions between graphenic carbon and antioxidants leading to ROS production have also been suggested (Liu et al. 2011). In addition, GO can generate ROS in water under both UV and visible light conditions (Du et al. 2018). Due to their two-dimensional geometry and highly hydrophobic surface area, GFNs can interact with membrane lipids and induce direct physical toxicity (Hu et al. 2011; Sanchez et al. 2011) GO has also been shown to induce inflammatory responses (Chen et al. 2012; Wang et al. 2011) and mitochondrial toxicity (Zhang et al. 2012; Zhang et al. 2010). Physical contact of sharp GO edges with cellular membranes and components could result in injury-induced inflammation (Khan et al. 2019) and subsequent ROS production (Chen et al. 2016). Further, GO-associated increases in intracellular ROS (Lammel and Navas 2014) can overwhelm the antioxidant machinery and result in damage to mitochondria, DNA, lipids, and proteins. It is likely that upon GO exposure, both direct and indirect toxicity mechanisms contribute to oxidative damage, and multiple cellular processes lead to ROS production playing a primary role in the overall cellular adverse outcome. Based on the results from our current study as well as our 72 h exposure (Khan et al. 2019), we propose ROS-induced lipid peroxidation as a reliable biomarker and a key event in GO-induced toxicity. GO-induced mechanisms of ROS production are manifold (Shvedova et al. 2012), and further research is required to determine the specific nature of such cellular processes.

4.2.2 Glutathione-s-transferase—In comparison to our short-term (72 h) GO study where no significant changes in GST were found but some patterns of enzyme activity differences were observed (Khan et al. 2019), here we report elevated GST activities in gill and digestive gland tissues of oysters exposed to GO for 14 d. Changes in enzyme activities are often reported as values normalized to tissue protein levels, as shown in Figure 6B. Normalized GST data provide a better comparison between samples and a robust assessment of enzymatic response. Upregulation of stress enzymes, such as GST, is energy intensive and represents a long-term response to nanomaterial exposures. Although no current GFN toxicity information of this phase II detoxification enzyme is available for molluscs, a few studies have reported changes in GST activities in other organisms (De Marchi et al. 2017; Fernandes et al. 2018; Mesarič et al. 2015). However, our understanding of the nature of GST response to GO exposure in aquatic invertebrates remains limited. Similar to our results, GO-exposed polychaetes were shown to have elevated GST activities (De Marchi et al. 2017) but in contrast, a decline in GST activity was reported in exposed crustaceans (Mesarič et al. 2015). Such differences may represent changes in enzymatic activities that often undergo an increasing-decreasing (inverted U shaped) response curve, as seen in the digestive gland GST response (Figure 6) in the current study. Stress enzymes often show initial increases with increasing severity of exposure stress, followed by a decline either due to catabolic processes or the involvement of other compensatory mechanisms (Viarengo et al. 2007). Our GST biomarker data combined with the significantly high lipid peroxidation in GO-exposed oysters are indicative of sublethal toxicity and highlight the importance of assessing multiple molecular markers to evaluate nanomaterial effects.

In addition to biotransformation and detoxification of xenobiotics, GST is also implicated in altering glutathione levels during ROS-induced stress and apoptotic pathways (Tew and Ronai 1999). The role of GST enzyme family members, especially GSTp, in coordinated regulation of stress kinases has been reported in response to ROS-generation. Such regulation includes activation of p38, NFκB (nuclear factor kappa light chain enhancer of activated B cells), and ERK (extracellular receptor kinase) signaling cascades and inhibition of JNK (Jun N-terminal kinase) signaling. Generation of ROS also activates GST transcription via JNK/Jun cascade and is thought to be responsible for the redox-dependent feedback loop of stress kinases (Yin et al. 2000). The balance between these kinases and signaling cascades is a key determinant of cellular health and fate. Further, according to the hierarchical oxidative stress model of nanomaterial toxicity (Nel et al. 2006), adverse outcomes such as cell death and apoptosis are preceded by induction of phase II enzymes, such as GSTs, and ROS-dependent activation of transcription factors.

4.2.3 Total protein—The total protein levels were found to be unaffected by 14 d of GO exposures in the current study. As expected, gill total protein levels were lower than digestive gland tissues, which represents a tissue-specific baseline biochemical difference. Our short term 72 h study (Khan et al. 2019) showed declines in total digestive gland protein levels at the exposure concentration of 1 mg/L GO. These contrasting results emphasize the differences between short- and long-term response patterns that must be taken into consideration for nanotoxicity evaluation.

4.3 Development of graphene oxide AOP

Based on our results, we propose that elevated oxidative lipid damage and GST-dependent signaling play integral roles in the AOP for GO that may lead to cell death. (Figure 8). We have previously also reported that cellular damage and death could be a histopathological outcome of GO exposures (Khan et al. 2019). Figure 8 outlines a diagrammatic representation of the conceptual use of current information available, from our studies as well as those of others, regarding the effects of GO exposures towards the overall goal of contributing to the process of AOP development. Interactions of GO at the cell surface, including endo-/phago-cytotic uptake, direct piercing of the plasma membrane, and generation of ROS at the cell surface, are potential initiating events (IEs). Other studies have also suggested such GO-associated events (Hu et al. 2015; Katsumiti et al. 2017; Mu et al. 2012), but further work is required to evaluate uptake and accumulation of GO using *in vivo* studies with marine organisms. Excessive intracellular production of ROS is most likely the first key event (KE1) that leads to damage to PUFAs (Kelly et al. 1998), represented by elevated MDA levels in our lipid peroxidation results. Lipid peroxidation is a self-propagating and self-sustaining process with several oxidation products that further generate ROS. Among these products, MDA and HNE play an important role in DNA and protein adduct formation and subsequent damage as well as in signal transduction pathways (Nam 2011). Based on the results from our GO studies, lipid peroxidation and oxidative damage to other macromolecules and organelles induced by ROS is proposed as the second key event in this AOP (KE2). Induction of antioxidant enzymes such as superoxide dismutase and catalase in response to GO exposures suggesting excessive ROS production has also been reported by others (Chen et al. 2016; De Marchi et al. 2017; Hu et al. 2015). Although not evaluated in the current study, mitochondrial membrane permealization and subsequent signaling cascades could contribute to this AOP. Mitochondrial membrane permealization associated with elevated ROS and induction of apoptosis via signaling pathways have been suggested in graphene studies with mammalian cell lines (Li et al. 2012; Wang et al. 2013; Zhang et al. 2010). ROS-associated changes in GST activities resulting in activation of cellular signaling (KE3) are integral to our understanding of the overlap between detoxification, antioxidant potential, and signaling mechanisms of phase II enzymes in nanomaterial toxicity. In recent literature, the role of GSTs as significant regulators of cell survival and proliferation pathways has emerged (Board and Menon 2013; Pajaud et al. 2012). As discussed previously, in its non-catalytic regulatory role under elevated ROS conditions, GSTp isozyme is involved in a signaling cascade due to protein-protein interactions with kinases that eventually results in apoptosis (Kalinina et al. 2014; Tew and Townsend 2012). Further, GSTs play a critical role in redox-dependent processes and glutathione metabolism which are associated with cellular antioxidant potential and susceptibility to oxidative stress (Kalinina et al. 2014). Although the underlying mechanisms are not fully understood, such changes in GST activity, as seen in our study, highlight the critical role that redox-signaling and regulatory kinases can play in graphene toxicity. Future investigations into the role of ROS as a second messenger in signaling cascades and non-catalytic functions of detoxification enzymes will assist in developing these key event relationships (KERs) for the proposed AOP. It must be noted that cell death (KE4) is most likely an outcome of multiple simultaneously-active mechanisms and other carbon nanomaterials have been shown to cause apoptotic as well as necrotic cell death (De Stefano

et al. 2012). Further characterization of cell death and related molecular events and markers is required to better understand nanomaterial-induced cellular adverse effects.

It must also be noted that based on our results, both digestive gland and gills are target tissues for GO-induced cellular oxidative damage and changes in enzymatic activities. Tissue damage, potential induction of stress signaling, and apoptotic pathways in both tissues can affect multiple physiological processes leading to AOs. Gills are the primary food and particle capture organs in oysters and their damage could impact food capture and respiration, whereas digestive gland damage could affect digestion, assimilation and nutritional status (McCarthy et al. 2013). Such tissue-specific changes can potentially assist in understanding AOs at higher level of organization, such as reduced growth, fitness, and survival. Apoptotic and oxidative stress responses along with organ-specific effects of GO have been described in a zebrafish study (Souza et al. 2017). However, such individual-level effects of GO exposures in aquatic organisms need further investigations towards the overall goal of AOP development. In conclusion, our static renewal studies provide new information on GO toxicity in marine bivalves. These *in vivo* studies identify a cellular damage marker as well as an enzyme marker for AOP development and suggest oxidative stress and associated signaling as putative mechanisms of GO-related environmental risks. With a rapidly growing GFN consumer market, there is an urgent need to expand on our knowledge of marine exposures and associated stress responses especially to economically-important organisms like oysters.

Supplementary Material

Refer to Web version on PubMed Central for supplementary material.

Acknowledgements

The authors would like to acknowledge L. Mills, M. Cashman, and B. Clark for their contributions towards the review of this manuscript. We would also like to thank Perry Raso for the oysters. This research was performed while B. Khan held an NRC Research Associateship award at the U.S. EPA, ORD/NHEERL, Atlantic Ecology Division.

Funding

This research was supported by the National Research Council under the Research Associateship Programs (Associate ID A1431000).

References

Adeleye AS, Conway JR, Garner K, Huang Y, Su Y, Keller AA. 2016 Engineered nanomaterials for water treatment and remediation: Costs, benefits, and applicability. Chemical Engineering Journal 286:640–662.

Adeleye AS, Ho KT, Zhang M, Li Y, Burgess RM. 2019 Fate and transformation of graphene oxide in estuarine and marine waters. Environmental Science & Technology 53:5858–5867. [PubMed: 30998850]

Ahmed F, Rodrigues DF. 2013 Investigation of acute effects of graphene oxide on wastewater microbial community: A case study. Journal of Hazardous Materials 256–257:33–39.

Ankley GT, Bennett RS, Erickson RJ, Hoff DJ, Hornung MW, Johnson RD, et al. 2010 Adverse outcome pathways: A conceptual framework to support ecotoxicology research and risk assessment. Environmental Toxicology and Chemistry 29:730–741. [PubMed: 20821501]

Awasthi YC, Yang Y, Tiwari NK, Patrick B, Sharma A, Li J, et al. 2004 Regulation of 4-hydroxynonenal-mediated signaling by glutathione s-transferases. Free Radical Biology and Medicine 37:607–619. [PubMed: 15288119]

Bitounis D, Ali-Boucetta H, Hong BH, Min DH, Kostarelos K. 2013 Prospects and challenges of graphene in biomedical applications. Advanced Materials 25:2258–2268. [PubMed: 23494834]

Board PG, Menon D. 2013 Glutathione transferases, regulators of cellular metabolism and physiology. Biochimica et Biophysica Acta (BBA) - General Subjects 1830:3267–3288. [PubMed: 23201197]

Canesi L, Ciacci C, Fabbri R, Marcomini A, Pojana G, Gallo G. 2012 Bivalve molluscs as a unique target group for nanoparticle toxicity. Marine Environmental Research 76:16–21. [PubMed: 21767873]

Canesi L, Corsi I. 2016 Effects of nanomaterials on marine invertebrates. Science of the Total Environment 565:933–940. [PubMed: 26805446]

Chae YJ, Pham CH, Lee J, Bae E, Yi J, Gu MB. 2009 Evaluation of the toxic impact of silver nanoparticles on japanese medaka (oryzias latipes). Aquatic Toxicology 94:320–327. [PubMed: 19699002]

Chang Y, Yang S-T, Liu J-H, Dong E, Wang Y, Cao A, et al. 2011 In vitro toxicity evaluation of graphene oxide on a549 cells. Toxicology letters 200:201–210. [PubMed: 21130147]

Chen G-Y, Yang H-J, Lu C-H, Chao Y-C, Hwang S-M, Chen C-L, et al. 2012 Simultaneous induction of autophagy and toll-like receptor signaling pathways by graphene oxide. Biomaterials 33:6559–6569. [PubMed: 22704844]

Chen M, Yin J, Liang Y, Yuan S, Wang F, Song M, et al. 2016 Oxidative stress and immunotoxicity induced by graphene oxide in zebrafish. Aquatic Toxicology 174:54–60. [PubMed: 26921726]

Chowdhury I, Duch MC, Mansukhani ND, Hersam MC, Bouchard D. 2013 Colloidal properties and stability of graphene oxide nanomaterials in the aquatic environment. Environmental Science & Technology 47:6288–6296. [PubMed: 23668881]

De Marchi L, Neto V, Pretti C, Figueira E, Brambilla L, Rodriguez-Douton MJ, et al. 2017 Physiological and biochemical impacts of graphene oxide in polychaetes: The case of *diopatra neapolitana*. Comparative Biochemistry and Physiology Part C 193:50–60. [PubMed: 28111252]

De Stefano D, Carnuccio R, Maiuri MC. 2012 Nanomaterials toxicity and cell death modalities. Journal of Drug Delivery 2012:14.

Du T, Adeleye AS, Zhang T, Jiang C, Zhang M, Wang H, et al. 2018 Influence of light wavelength on the photoactivity, physicochemical transformation, and fate of graphene oxide in aqueous media. Environmental Science: Nano 5:2590–2603.

Fernandes AL, Nascimento JP, Santos AP, Furtado CA, Romano LA, da Rosa CE, et al. 2018 Assessment of the effects of graphene exposure in danio rerio: A molecular, biochemical and histological approach to investigating mechanisms of toxicity. Chemosphere 210:458–466. [PubMed: 30025363]

Goodwin J, David G, Adeleye AS, Sung L, Ho KT, Burgess RM, Petersen EJ. 2018 Detection and quantification of graphene-family nanomaterials in the environment. Environmental Science & Technology 52:4491–4513. [PubMed: 29505723]

Guo X, Mei N. 2014 Assessment of the toxic potential of graphene family nanomaterials. Journal of Food and Drug Analysis 22:105–115. [PubMed: 24673908]

Hu W, Peng C, Lv M, Li X, Zhang Y, Chen N, et al. 2011 Protein corona-mediated mitigation of cytotoxicity of graphene oxide. ACS NANO 5:3693–3700. [PubMed: 21500856]

Hu X, Ouyang S, Mu L, An J, Zhou Q. 2015 Effects of graphene oxide and oxidized carbon nanotubes on the cellular division, microstructure, uptake, oxidative stress, and metabolic profiles. Environmental Science & Technology 49:10825–10833. [PubMed: 26295980]

Huang X, Yin Z, Wu S, Qi X, He Q, Zhang Q, et al. 2011 Graphene-based materials: Synthesis, characterization, properties, and applications. Small 7:1876–1902. [PubMed: 21630440]

Jastrzębska AM, Kurtycz P, Olszyna AR. 2012 Recent advances in graphene family materials toxicity investigations. Journal of Nanoparticle Research 14:1–20. [PubMed: 22448125]

Kalinina E, Chernov N, Novichkova M. 2014 Role of glutathione, glutathione transferase, and glutaredoxin in regulation of redox-dependent processes. Biochemistry (Moscow) 79:1562–1583. [PubMed: 25749165]

Katsumiti A, Tomovska R, Cajaraville MP. 2017 Intracellular localization and toxicity of graphene oxide and reduced graphene oxide nanoplatelets to mussel hemocytes in vitro. Aquatic Toxicology 188:138–147. [PubMed: 28521151]

Kelly K, Havrilla CM, Brady TC, Abramo KH, Levin ED. 1998 Oxidative stress in toxicology: Established mammalian and emerging piscine model systems. Environmental Health Perspectives 106:375–384. [PubMed: 9637794]

Khan B, Ringwood AH. 2016 Cellular biomarker responses to hypoxia in eastern oysters and atlantic ribbed marsh mussels. Marine Ecology Progress Series 546:123–133.

Khan B, Adeleye AS, Burgess RM, Smolowitz R, Russo SM, Ho KT. 2019 A 72-h exposure study with eastern oysters (crassostrea virginica) and the nanomaterial graphene oxide. Environmental Toxicology and Chemistry 38:820–830. [PubMed: 30667076]

Lammel T, Navas JM. 2014 Graphene nanoplatelets spontaneously translocate into the cytosol and physically interact with cellular organelles in the fish cell line plhc-1. Aquatic Toxicology 150:55–65. [PubMed: 24642293]

Lee JW, Won E-J, Raisuddin S, Lee J-S. 2015 Significance of adverse outcome pathways in biomarker-based environmental risk assessment in aquatic organisms. Journal of Environmental Sciences 35:115–127.

Li Y, Liu Y, Fu Y, Wei T, Le Guyader L, Gao G, et al. 2012 The triggering of apoptosis in macrophages by pristine graphene through the mapk and tgf-beta signaling pathways. Biomaterials 33:402–411. [PubMed: 22019121]

Liu X, Sen S, Liu J, Kulaots I, Geohegan D, Kane A, et al. 2011 Antioxidant deactivation on graphenic nanocarbon surfaces. Small 7:2775–2785. [PubMed: 21818846]

Lushchak VI. 2012 Glutathione homeostasis and functions: Potential targets for medical interventions. Journal of Amino Acids 2012:26.

McCarthy MP, Carroll DL, Ringwood AH. 2013 Tissue specific responses of oysters, *crassostrea virginica*, to silver nanoparticles. Aquatic Toxicology 138:123–128. [PubMed: 23728357]

Mesarič T, Gambardella C, Milivojević T, Faimali M, Drobne D, Falugi C, et al. 2015 High surface adsorption properties of carbon-based nanomaterials are responsible for mortality, swimming inhibition, and biochemical responses in *artemia salina* larvae. Aquatic Toxicology 163:121–129. [PubMed: 25889088]

Moore M 2006 Do nanoparticles present ecotoxicological risks for the health of the aquatic environment? Environment International 32:967–976. [PubMed: 16859745]

Mu Q, Su G, Li L, Gilbertson BO, Yu LH, Zhang Q, et al. 2012 Size-dependent cell uptake of protein-coated graphene oxide nanosheets. ACS Applied Materials & Interfaces 4:2259–2266. [PubMed: 22409495]

Nam T-G. 2011 Lipid peroxidation and its toxicological implications. Toxicol Res 27:1–6. [PubMed: 24278542]

Nel A, Xia T, Mädler L, Li N. 2006 Toxic potential of materials at the nanolevel. Science 311:622–627. [PubMed: 16456071]

Novoselov KS, Fal V, Colombo L, Gellert P, Schwab M, Kim K. 2012 A roadmap for graphene. Nature 490:192–200. [PubMed: 23060189]

Pajaud J, Kumar S, Rauch C, Morel F, Aninat C. 2012 Regulation of signal transduction by glutathione transferases. International Journal of Hepatology 2012:11.

Qi K, Sun Y, Duan H, Guo X. 2015 A corrosion-protective coating based on a solution-processable polymer-grafted graphene oxide nanocomposite. Corrosion Science 98:500–506.

Regoli F, Principato G. 1995 Glutathione, glutathione-dependent and antioxidant enzymes in mussel, *mytilus galloprovincialis,* exposed to metals under field and laboratory conditions: Implications for the use of biochemical biomarkers. Aquatic Toxicology 31:143–164.

Sanchez VC, Jachak A, Hurt RH, Kane AB. 2011 Biological interactions of graphene-family nanomaterials: An interdisciplinary review. Chemical Research in Toxicology 25:15–34. [PubMed: 21954945]

Sayes CM, Gobin AM, Ausman KD, Mendez J, West JL, Colvin VL. 2005 Nano-c60 cytotoxicity is due to lipid peroxidation. Biomaterials 26:7587–7595. [PubMed: 16005959]

Shi J, Karlsson HL, Johansson K, Gogvadze V, Xiao L, Li J, et al. 2012 Microsomal glutathione transferase 1 protects against toxicity induced by silica nanoparticles but not by zinc oxide nanoparticles. ACS NANO 6:1925–1938. [PubMed: 22303956]

Shvedova AA, Pietroiusti A, Fadeel B, Kagan VE. 2012 Mechanisms of carbon nanotube-induced toxicity: Focus on oxidative stress. Toxicology and Applied Pharmacology 261:121–133. [PubMed: 22513272]

Souza JP, Baretta JF, Santos F, Paino IMM, Zucolotto V. 2017 Toxicological effects of graphene oxide on adult zebrafish (danio rerio). Aquatic Toxicology 186:11–18. [PubMed: 28242497]

Tew KD, Ronai Ze. 1999 Gst function in drug and stress response. Drug Resistance Updates 2:143–147. [PubMed: 11504484]

Tew KD, Townsend DM. 2012 Glutathione-s-transferases as determinants of cell survival and death. Antioxidants & Redox Signaling 17:1728–1737. [PubMed: 22540427]

Viarengo A, Lowe D, Bolognesi C, Fabbri E, Koehler A. 2007 The use of biomarkers in biomonitoring: A 2-tier approach assessing the level of pollutant-induced stress syndrome in sentinel organisms. Comparative Biochemistry and Physiology Part C 146:281–300. [PubMed: 17560835]

Volz DC, Belanger S, Embry M, Padilla S, Sanderson H, Schirmer K, et al. 2011 Adverse outcome pathways during early fish development: A conceptual framework for identification of chemical screening and prioritization strategies. Toxicological Sciences 123:349–358. [PubMed: 21750347]

Wang A, Pu K, Dong B, Liu Y, Zhang L, Zhang Z, et al. 2013 Role of surface charge and oxidative stress in cytotoxicity and genotoxicity of graphene oxide towards human lung fibroblast cells. Journal of Applied Toxicology 33:1156–1164. [PubMed: 23775274]

Wang K, Ruan J, Song H, Zhang J, Wo Y, Guo S, et al. 2011 Biocompatibility of graphene oxide. Nanoscale Research Letters 6:8–8. [PubMed: 27502632]

Wang Y, Wu S, Zhao X, Su Z, Du L, Sui A. 2014 In vitro toxicity evaluation of graphene oxide on human rpmi 8226 cells. Bio-Medical Materials and Engineering 24:2007–2013. [PubMed: 25226897]

Ward JE, Kach DJ. 2009 Marine aggregates facilitate ingestion of nanoparticles by suspension-feeding bivalves. Marine Environmental Research 68:137–142. [PubMed: 19525006]

Yin Z, Ivanov VN, Habelhah H, Tew K, Ronai Ze. 2000 Glutathione s-transferase p elicits protection against h2o2-induced cell death via coordinated regulation of stress kinases. Cancer Research 60:4053–4057. [PubMed: 10945608]

Yozzo KL, McGee SP, Volz DC. 2013 Adverse outcome pathways during zebrafish embryogenesis: A case study with paraoxon. Aquatic Toxicology 126:346–354. [PubMed: 23046524]

Zhang W, Wang C, Li Z, Lu Z, Li Y, Yin JJ, et al. 2012 Unraveling stress- induced toxicity properties of graphene oxide and the underlying mechanism. Advanced Materials 24:5391–5397. [PubMed: 22927326]

Zhang Y, Ali SF, Dervishi E, Xu Y, Li Z, Casciano D, et al. 2010 Cytotoxicity effects of graphene and single-wall carbon nanotubes in neural phaeochromocytoma-derived pc12 cells. ACS nano 4:3181–3186. [PubMed: 20481456]

Zhu S, Luo F, Chen W, Zhu B, Wang G. 2017 Toxicity evaluation of graphene oxide on cysts and three larval stages of *artemia salina*. Science of the Total Environment 595:101–109. [PubMed: 28380404]

Highlights

- Graphene oxide (GO) exposures are associated with elevated lipid peroxidation in Eastern oysters
- 14-d GO exposures led to elevated activity of glutathione-s-transferase (GST) enzyme
- Oxidative damage and induction of GST-associated signaling are putative mechanisms of GO toxicity as well as key events in the proposed adverse outcome pathway
- Oyster gills and digestive glands are susceptible to GO-induced adverse effects

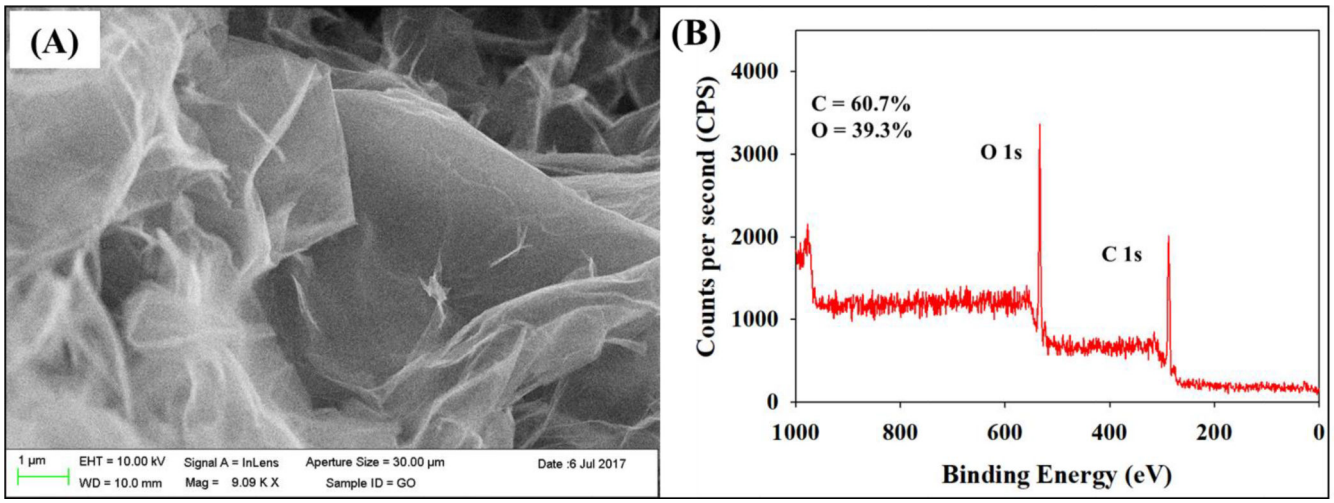

Figure 1.

Characterization of graphene oxide nanomaterial used in this study. (a) Scanning electron micrograph and (B) X-ray photoelectron spectroscopy survey scan showing atomic carbon and oxygen ratios.

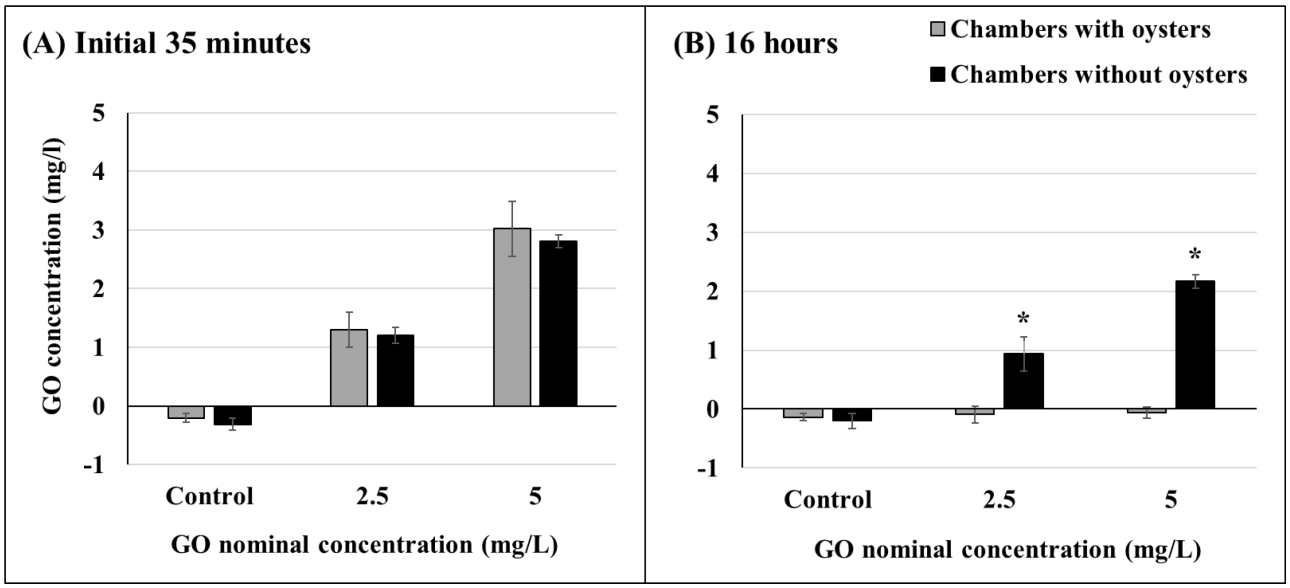

Figure 2.

Measured GO concentrations in chambers with and without oysters within the initial 35 minutes of GO addition (A) and 16 hours after GO addition (B). Asterisks represent significant differences between chambers with and without oysters. Initial 35 minutes: n = 10 for chambers with oysters, n = 5 for chambers without oysters; 16 hours: n = 8 for chambers with oysters, n = 4 for chambers without oysters. Values represent means and standard deviations.

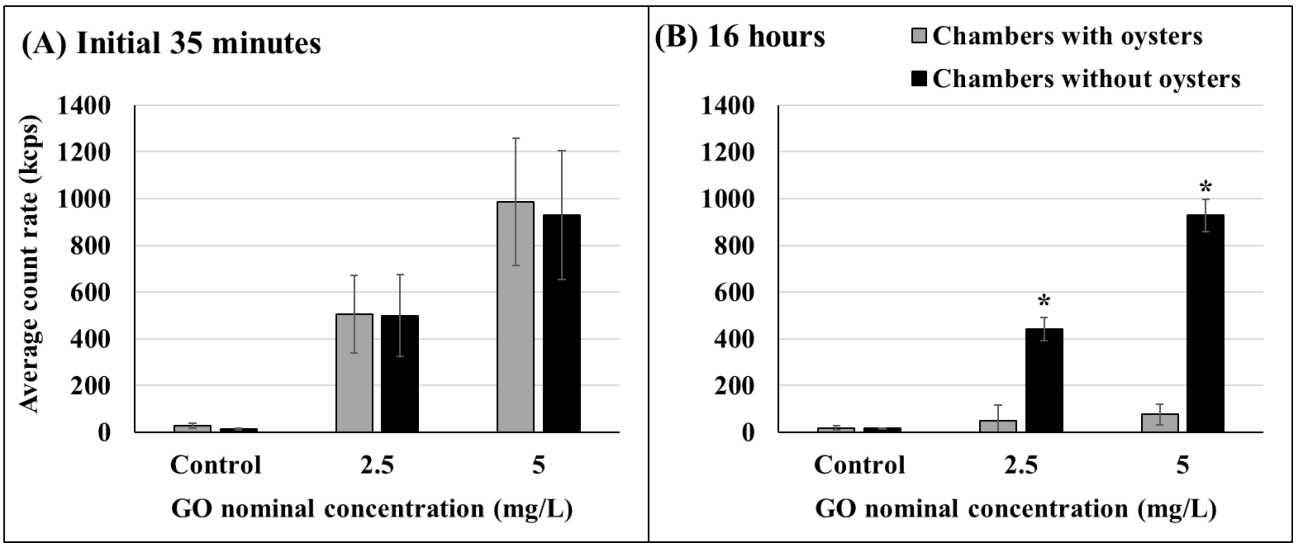

Figure 3.

Average particle count rate in chambers with and without oysters within the initial 35 minutes of GO addition (A) and 16 hours after GO addition (B). Asterisks represent significant differences between chambers with and without oysters. Initial 35 minutes: n = 10 for chambers with oysters, n = 5 for chambers without oysters; 16 hours: n = 8 for chambers with oysters, n = 4 for chambers without oysters. Values represent means and standard deviations.

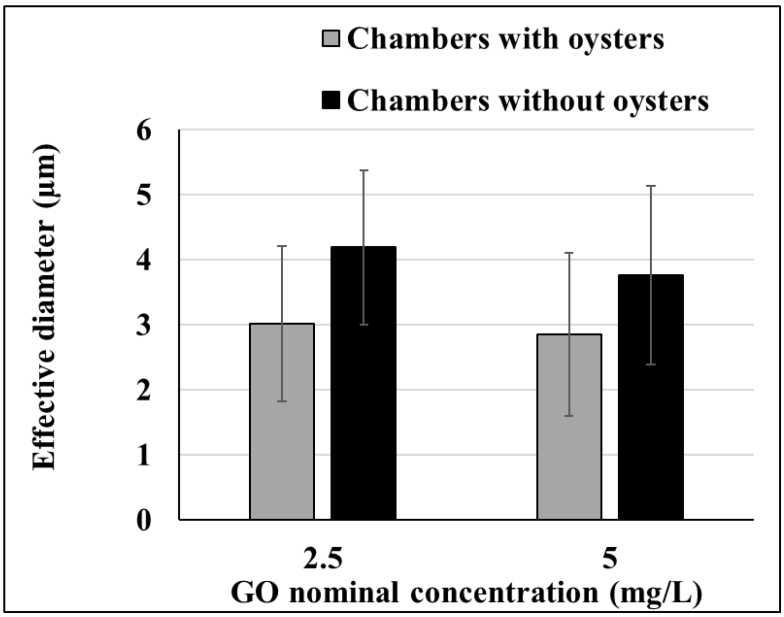

Figure 4.

Effective diameter assessments for chambers with and without oysters recorded within the initial 35 minutes of GO addition. No significant differences were observed, n = 7 for chambers with oysters, n = 5 for chambers without oysters. Values represent means and standard deviations.

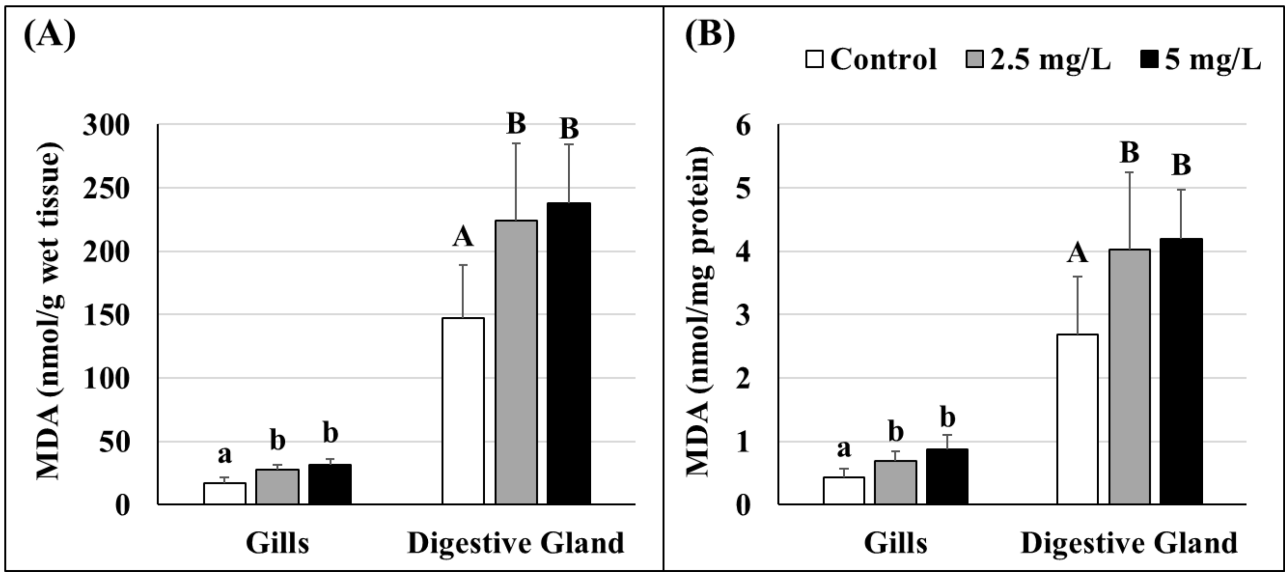

Figure 5.

Malondialdehyde (MDA) levels in gill and digestive gland tissues of control and GO-exposed oysters expressed as per gram wet tissue (A) and standardized per mg protein (B). Lowercase letters represent differences in gills and uppercase letters represent differences in digestive gland tissues of control and GO-exposed oysters. Different letters indicate significant differences between concentrations, n = 8 per treatment. Values represent means and standard deviations.

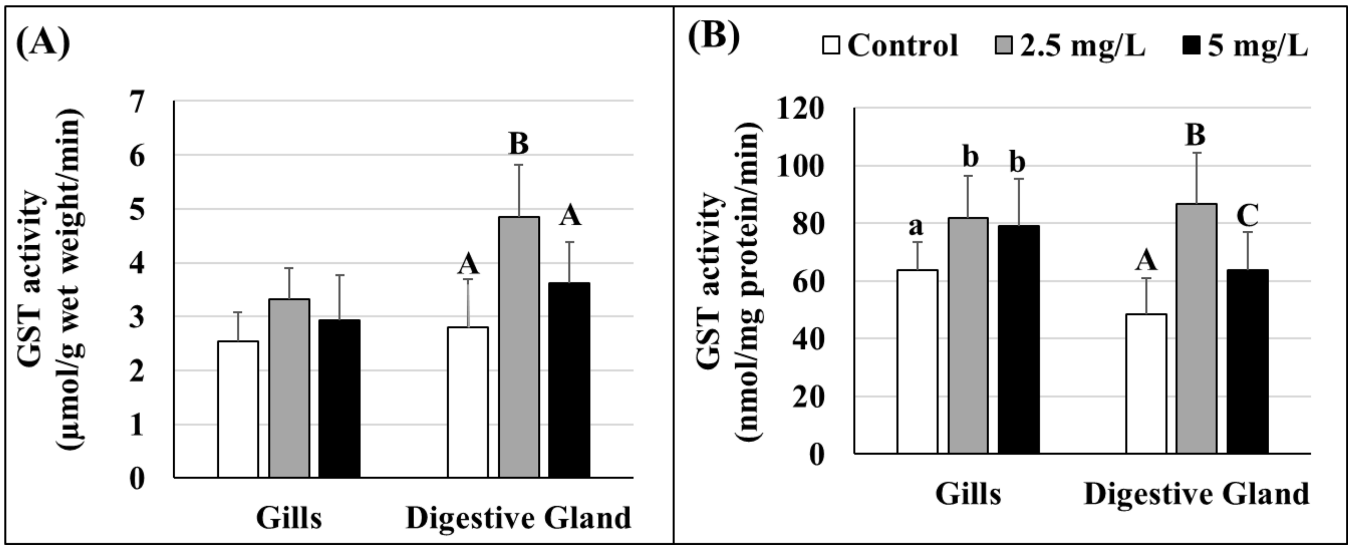

Figure 6.

Activity of glutathione-s-transferase (GST) in gill and digestive gland tissues of control and GO-exposed oysters expressed as per gram wet tissue (A) and standardized per mg protein (B). Lowercase letters represent differences in gills and uppercase letters represent differences in digestive gland tissues of control and GO-exposed oysters. Different letters indicate significant differences between concentrations, no letters represent no differences, n = 8 per treatment. Values represent means and standard deviations.

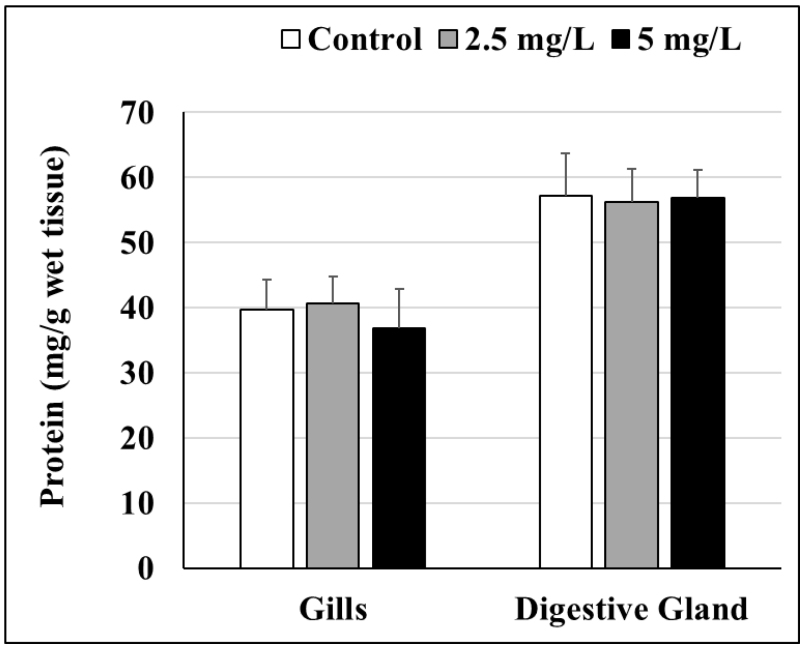

Figure 7.

Total protein levels in gill and digestive gland tissues of control and GO-exposed oysters. No significant differences were observed, n = 8. Values represent means and standard deviations.

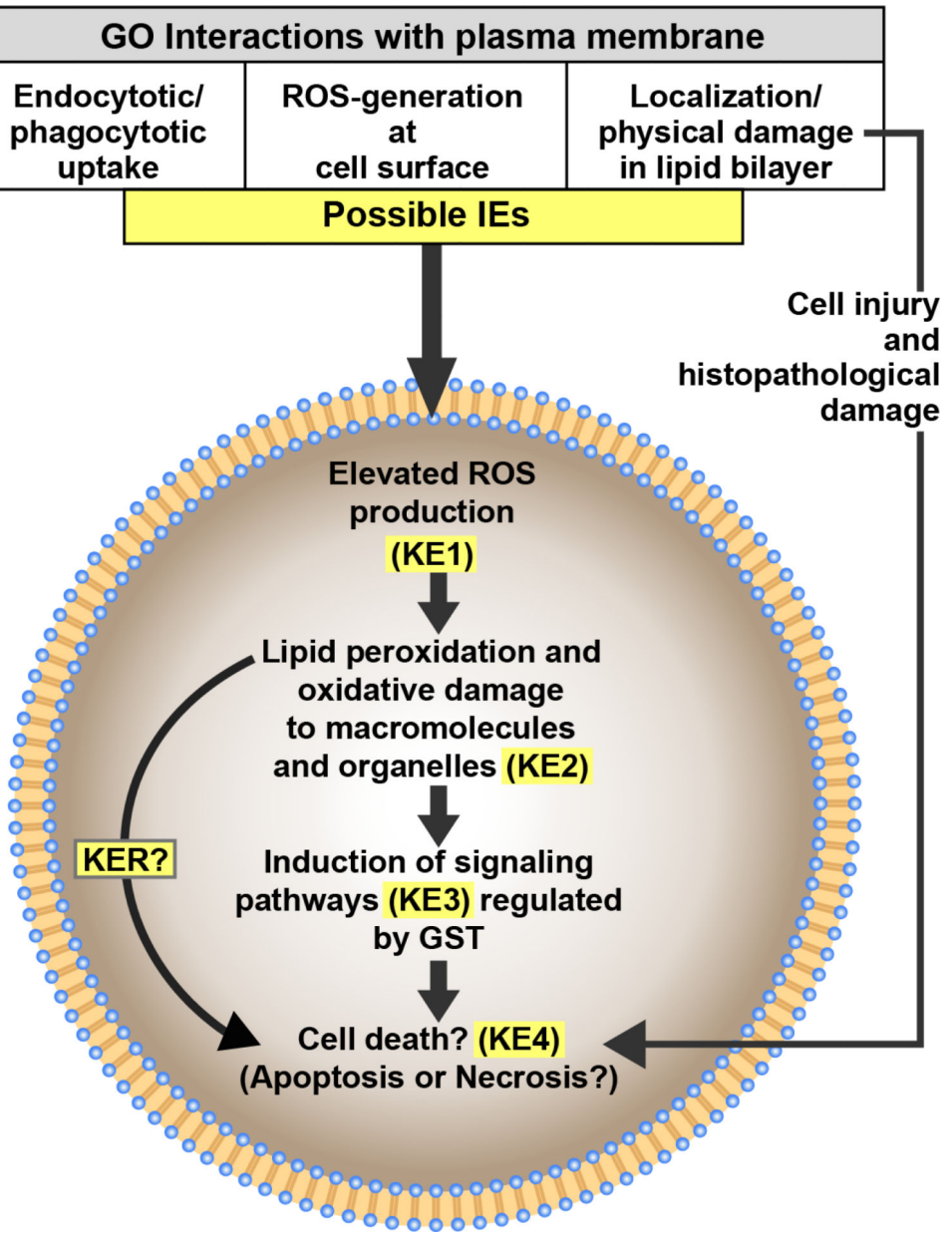

Figure 8.

Diagrammatic representation of the conceptual use of biomarker responses to GO in Eastern oysters (*Crassostrea virginica*) to identify cellular and subcellular key events towards the goal of contributing to the development of a potential nanomaterial Adverse Outcome Pathway (AOP). IE = Initiating Event, KE = Key Event, KER = Key Event Relationship.

Table 1.

Information on GO concentration and particle size from 5 mg/L GO chambers (A) and 2.5 mg/L GO chambers (B). For DLS measurements, the most abundant particle size is assigned a relative number of 100. Size distribution is shown as a range associated with particles assigned a relative number of at least 1 (frequency >1) and as a range associated with particles assigned any number > 0 (all data). Exposure chambers indicated as SW are seawater chambers without oysters.

A (5 mg/L)				**Size range (relative distribution)**		
Chamber #	**Time post GO addition**	**Conc.**	**Most abundant size**	**Frequency >1**	**All data**	**Effective diameter**
	(mins)	**(mg/L)**	**(nm)**	**(nm)**	**(nm)**	**(nm)**
1	2	3.23	68	68–94	68–8466	2183.8
7	2	3.11	130	130–210	130–3362	1803.1
13	2	3.86	183	183–1731	183–10,000	2414
19	2	3.49	316	258–1971	258–3278	1994.7
4	13	2.58	85	85–140	85–10,000	3528.3
10	13	3.20	94	94–763	94–10,000	2620.4
25 (SW)	21	2.70	132	132–1326	132–10,000	4444.3
25 (SW)	22	2.97	135	135–201	135–4889	3098.3
25 (SW)	23	2.73	103	103–499	103–6230	2892.9
25 (SW)	25	2.75	83	83–115	83–10,000	5835.9
B (2.5 mg/L)						
8	6	1.48	101	101–687	101–5419	1947.8
14	6	1.59	103	103–183	103–3303	1725.3
20	6	1.47	69	69–96	69–10,000	2232.8
5	17	1.04	107	107–147	107–10,000	4539.9
11	17	1.52	73	73–102	73–10,000	2944.8
17	17	1.05	106	106–169	106–10,000	2967.4
26 (SW)	24	1.26	83	83–156	83–10,000	4048.5
26 (SW)	26	1.19	114	114–153	114–4500	3434.2
26 (SW)	27	1.28	160	160–289	160–10,000	4000.6
26 (SW)	28	1.29	743	743–1081	743–10,000	6213.3